Journal of Research and Applications in Mechanical Engineering
ISSN: 2229-2152 (Print); 2697-424x (Online)
(2024) Vol. 12, No. 1, Paper No. JRAME-24-12-010
[DOI: 10.14456/jrame.2024.10]

Research Article

Efficiency Evaluation on Cooling Behavior of Water-Cooling Jacket for Synchronous Reluctance Motor

K.H. Nguyen[1]
M. Masomtob[2,*]
B. Kerdsup[3]
S. Karukanan[3]
P. Champa[3]
T.D. Pham[1]
S. Hirai[4]
C.T. Vo[5]
P. Kummool[6]
C. Charoenphonphanich[1]
[1] *Department of Mechanical Engineering, School of Engineering, King Mongkut's Institute of Technology Ladkrabang, Bangkok, 10520, Thailand*
[2] *National Energy Technology Center, National Science and Technology Development Agency, Pathum Thani, 12120, Thailand*
[3] *National Electronics and Computer Technology Center, National Science and Technology Development Agency, Pathum Thani, 12120, Thailand*
[4] *School of Engineering, Tokyo Institute of Technology, Tokyo, 152-8552, Japan*
[5] *Faculty of Automotive Engineering Technology, Industrial University of Ho Chi Minh City, Ho Chi Minh City, 727900, Vietnam*
[6] *International Academy of Aviation Industry, King Mongkut's Institute of Technology Ladkrabang, Bangkok, 10520, Thailand*

Received 30 August 2023
Revised 13 November 2023
Accepted 22 November 2023

Abstract:
This study presents the cooling efficiency after installing a water-cooling jacket for a 3-kW synchronous reluctance motor of an electric motorcycle and the factors influencing its thermal behavior by experimental and simulation approaches. The testing process was conducted as a method to collect input parameters and validate the results of the computing simulation. The simulation procedure used the step running technique to evaluate two different water-path models. The findings indicated that the maximum temperature of the stator winding and jacket cover decreased by 19.12 °C and 16.07 °C, respectively, following the installation of the water jacket and operation at a low flow rate with a current supply of 200 A. Furthermore, increasing the water flow rate leads to a substantial decrease in maximum temperature before a certain flow rate; 2 liters per minute (LPM) was chosen as the optimal rate. Temperature fluctuations exhibit an upward trend up to 1.85 °C with the higher supplied currents but drop with a higher flow rate. In addition, the motor maximum temperature in the long water-path jacket (LWJ) model was lower than in the short water-path jacket (SWJ) model due to the higher heat transfer coefficient (HTC).

Keywords: *Synchronous reluctance motor, Electric motorcycle, Water-Cooling jacket, Time-Dependent temperature*

1. Introduction

Facing the depletion risk of fossil fuel resources, the world's attitude towards the internal combustion engine has changed. Given this situation, electric vehicle (EVs) was being considered as a potential replacement for vehicles powered by ICE [1]. The current state of EVs still offers opportunities for improvement, with vehicle performance being a central focus of research and development efforts [2-4]. According to Wang et al. [5], high power density in

* Corresponding author: M. Masomtob
E-mail address: manop.mas@entec.or.th

motor design leads to an increase in loss density, making thermal management more challenging and becoming a significant obstacle to efficiency. Managing the temperature parameters of EV motors was an unavoidable challenge that must be addressed to achieve widespread adoption of EVs in the future.

There are various methods for controlling the motor temperature of electric vehicles, but the three most commonly used methods are air cooling, oil cooling, and water cooling. Air cooling has long been recognized as a simple and fundamental method for various electric machines utilizing thermal sinks. Because the efficiency of the air-cooling approach using thermal sinks under harsh working conditions was low, this method has undergone several improvements. Specifically, the technique of directing air into air gaps along the rotor shaft and motor housing was researched by Kim et al. [6]. However, this cooling technique necessitates significant alterations to the original motor structure. Another air-cooling study was conducted by Prieto et al. [7], which did not require motor modification, but airflow was controlled forcibly by a fan; subsequently, hot air was cooled by a water jacket. On the other hand, oil cooling, a popular option, was studied by Marcolini et al. [8], who conducted a comparative and evaluative study between direct oil cooling of end-windings and a water jacket. The experimental results demonstrated direct oil-cooled coils could extract up to 2.87 times the amount of heat compared to indirect water cooling. In addition, Gundabattini et al. [9], in their study, also concluded that the highest cooling performance was achieved by direct oil cooling, followed by water cooling, and finally, air cooling. The study also indicated that the air-cooling and the water-cooling exhibit cooling uniformity, while the oil cooling does not. The above air-cooling and oil-cooling processes require modifications to the original motor structure, which affects stress, strain, and deformation during operation by manufacturers. Therefore, the study of a water-cooling jacket (WJ) was preferred due to its uniform cooling, average cooling performance, and the ability to be installed as an extra component without affecting the motor's structure [10-13]. Moreover, the study by Nategh et al. [14] emphasized the dominance of utilizing the water-cooling system in synchronous reluctance machines, particularly in minimizing the temperature difference between the shaft and the inner part of the stator teeth due to the effective heat transfer process. In another study, Herrera et al. [15] employed a liquid cooling system for synchronous reluctance motor design based on an EVs powertrain.

In this study, the water-cooling jacket serves not only as a cooling function but also as a method to determine the heat generation of the motor. Additionally, the research assesses the impact of cooling process factors such as water flow rate, water jacket path, and supply current on maximum temperature, temperature fluctuation, and temperature distribution.

2. Numerical Methodology

2.1 Experimental Setup and Simulation Validation

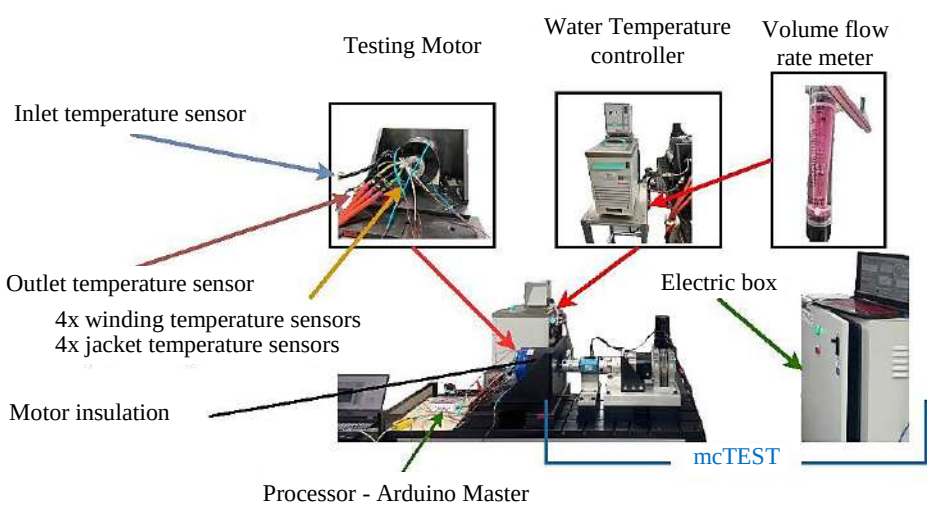

Fig. 1. Experimental validation setup.

Two models of cooling jackets were predicted and analyzed based on FEM. In order to evaluate the accuracy of the simulation results, an experimental setup for validation was built, as depicted in Fig. 1. The experimental setup consists of a motor characteristic testbed (mcTEST) [16], synchronous reluctance motor (SynRM) with a water-cooling jacket and a water temperature controller. The mcTEST was a statistical testing method used to determine the torque of a motor based on the supplied current. This testing process generates heat corresponding to different motor torques. Consequently, the cooling process was applied for experiment and evaluation.

In addition to validation, this process was used for collecting data to be utilized as input parameters for the simulation process, such as heat generation, volume flow rate, and inlet temperature, as described in Eq. (1) [17].

$$Q = F_v \times \rho \times C_p \times (T_{outlet} - T_{inlet}) \tag{1}$$

The short water-path jacket has been built to verify the effective cooling capacity of the cooling jacket. Temperature measurements were collected from four different positions inserted in the stator winding and the WJ, labelled as T_1, T_2, T_3, T_4 and T_5, T_6, T_7, T_8 respectively, as shown in Fig. 2 and Fig. 3. These positions were strategically located along the water channel's circulation path of SWJ. The temperature distribution was expected to increase gradually from T_1 to T_4 and from T_5 to T_8. The Arduino master processor was used for collecting, processing temperature sensor signals, and transmitting them to the LabVIEW platform via the serial port for display and data export. The outer part of the jacket was covered with three layers of insulation, as shown in Fig. 4. This cover aims to ensure that the heat generated by the motor was only removed by the WJ, without the influence of the ambient temperature. Moreover, the heat transfer coefficient (HTC) of the WJ can be determined with greater ease and accuracy under these conditions.

$$HTC = \frac{q}{T_{inside} - T_{outside}} \tag{2}$$

$$q = \frac{Q}{A} \tag{3}$$

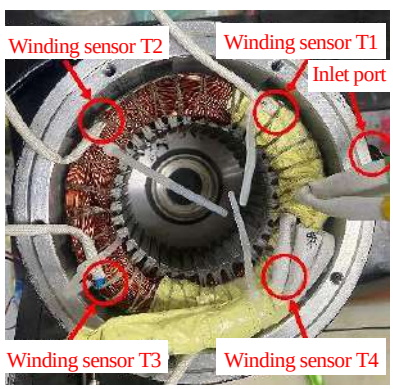

Fig. 2. Locations of winding temperature sensors.

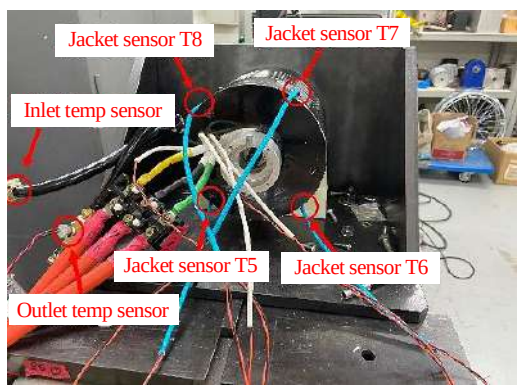

Fig. 3. Locations of water jacket temperature sensor.

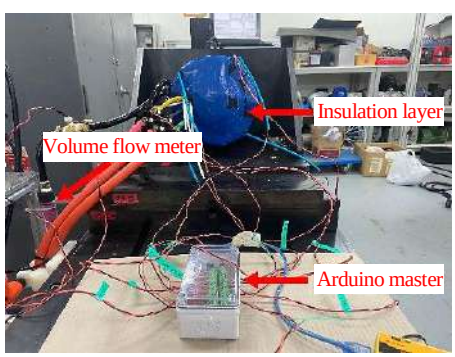

Fig. 4. Installation of thermal insulation layer.

2.2 Mesh Specification

Mesh quality was a crucial parameter that impacts the accuracy of FEM results [18]. To ensure the reliability of the simulation, the grid independence should be verified to eliminate influence of the grid on the computing accuracy [19]. The SWJ model was selected as the benchmark for assessing mesh quality. It utilized input parameters and boundary conditions illustrated in Fig. 5, which included the maximum motor heat generation of 119.63 W, the flow rate of 2.25 LPM, and the maximum inlet temperature of 24.45 °C. The effect of mesh on the maximum temperature of WJ depicted in Fig. 6, was divided into three different element numbers to facilitate comparative simulations. The maximum jacket temperatures of 28486 elements, 48936 elements, and 95244 elements were 25.7 °C, 25.53 °C, and 25.54 °C, respectively. The temperature difference between the last two element numbers was relatively minor, just 0.01 °C. Consequently, it can be observed that the simulation results were independent of the element number when there were more than 48936 elements. Therefore, the model with a mesh quality of 95244 elements was selected to conduct further calculations.

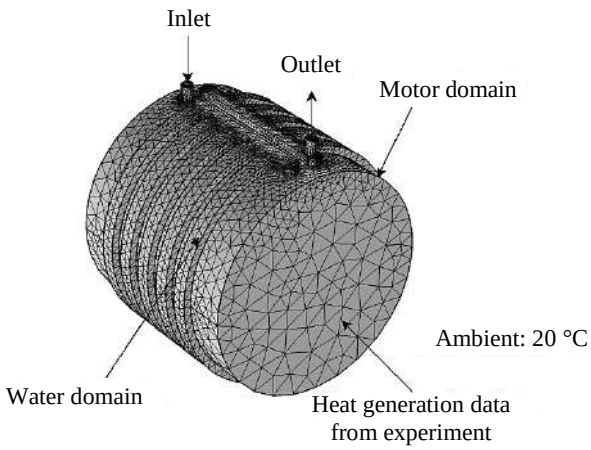

Fig. 5. Meshes of WJ concept.

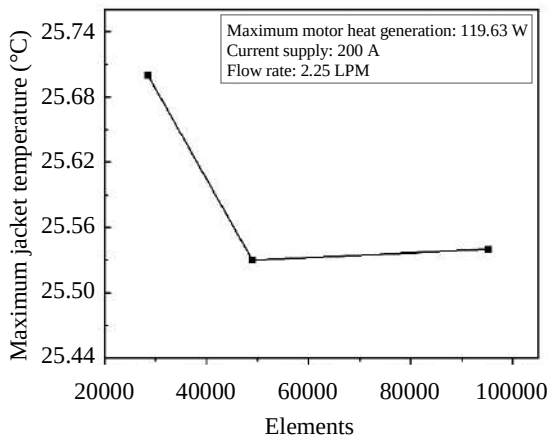

Fig. 6. Effect of mesh on the maximum temperature of WJ.

2.3 Step Simulation Running Technique

In this study, the water properties were maintained as constant values. So, the simulation process was conducted using a step running approach as described in Fig. 7. After inserting input parameters and meshing the WJ model, the step-running approach was employed to reduce computational load and minimize simulation time instead of running all components simultaneously. The computed results of the laminar flow component served as the initial condition, guiding the computation of the heat transfer component.

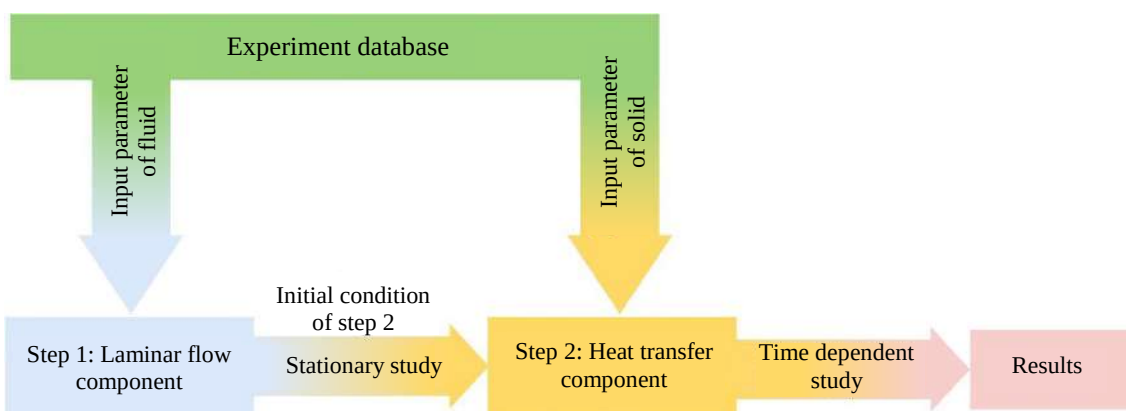

Fig. 7. Step running of simulation process.

3. Model Formulation

3.1 SynRM parameters

The SynRM of an electric motorcycle was utilized for researching the cooling system. The parameters of the motor were presented in Table 1. This motor type includes non-permanent magnetic poles on the ferromagnetic rotor, and the winding was not installed on the rotor. This implies that its torque was solely generated by magnetic reluctance. The mcTEST was suitable for cooling research and determining heat power losses since 97% of motor power losses originate directly from the winding and stator [13]. The installation process of the cooling jacket does not impact the original motor design; it was merely an additional component.

Table 1: Synchronous reluctance motor parameters.

Parameters	**Value**
Motor rated power	3 kW
Motor maximum power	5 kW
DC supply voltage	72 VDC
Motor nominal torque	5.7 Nm
Motor maximum torque	9.5 Nm
Max. efficiency	90 %
Max. stator current density	15 A/mm^2
Motor cooling type	Totally enclosed
Max. Motor operating temperature	130 ^{o}C

3.2 Comparison of Three Cooling Models

The WJ was designed with two components: a topology of water jacket and a jacket cover. As aforementioned, this type of cooling system was installed externally without altering the structure of the motor, as depicted in Fig. 8.

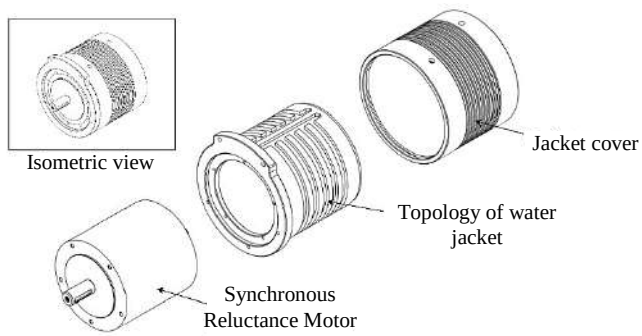

Fig. 8. Exploded view of motor-water jacket installation.

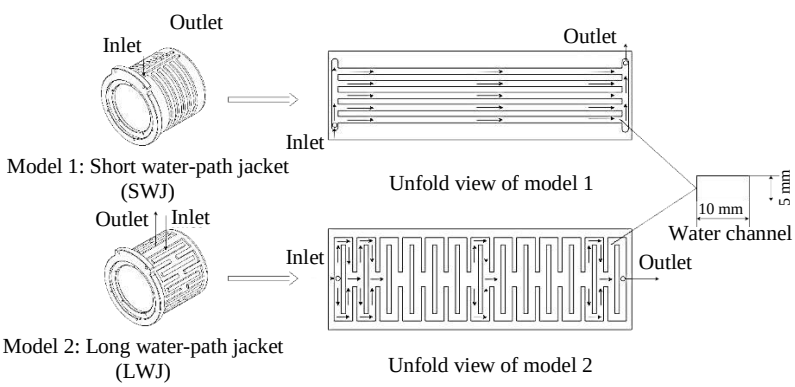

Fig. 9. Configurations of water jacket topology.

Apart from the laminar flow rate, the topology of the water jacket significantly impacts thermal behaviours during the cooling process. Fig. 9 showed two distinct topology characteristics of cooling jackets, namely the short water-path jacket and the long water-path jacket. In the SWJ configuration, five water channels were presented, with the water path following a circular route and the inlet and outlet channels positioned at the corners of the two main water channels. In the LWJ configuration, one primary water channel exists alongside two secondary water channels that alternate in combining and separating the flow, contributing to a more uniform water temperature distribution. Furthermore, the water path of the LWJ model alternates between circular and longitudinal routes, contributing to a more uniform cooling in every area. The inlet and outlet channels situated in the middle positions of the main water channel enable the flow to disperse to both sides, ensuring a consistent flow rate throughout the topology of the water jacket.

4. Results and Analysis

4.1 Simulation Validation via Experiment

Fig. 10 shows the time-dependent temperature graph of the SWJ between the experiment and simulation. Due to the substantial temperature fluctuations in the experimental results, the collected data underwent a filtering process to achieve a smoother representation. In the results, the temperature curve can be divided into two phases: an unstable phase and a stable phase.

Fig. 10 was explained by the law of conservation of energy. This graph is divided into Zone 1, Zone 2, and Zone 3, represented by the colors blue, green, and orange, respectively. During the initial phase, the chart was divided into Zone 1 and Zone 2. Zone 1 represents the heat absorption by the jacket material, aluminum. This heat absorption gradually decreases over time until it reaches a saturation state. Consequently, the heat absorption taken by the water in Zone 2 increases to offset the diminishing impact of the aluminum. This means that during the unstable phase of Fig. 10, the heat generation of the motor was absorbed simultaneously by the aluminum material and the flowing water inside. As the aluminum reaches its heat saturation state, the chart transitions into the stable phase. At this moment, the heat generation of the motor was solely removed by the water. This implies that the heat absorbed by the water corresponds to the heat generation of the motor, as demonstrated in Zone 3. According to the results, it can be observed that the temperature behavior of the simulation and experimental filter tends to be similar to each other in both stable and unstable phase.

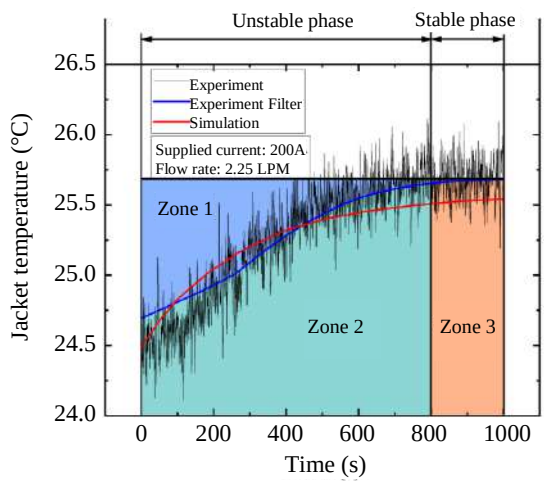

Fig. 10. Jacket temperature comparison between simulation and experiment.

4.2 The Effectiveness of Water-Cooling Jacket

In Fig. 11 and 12, the experimental results have demonstrated the effective thermal behaviour of the motor after combining with the WJ. With a supplied current of 200 A, as the flow rate increased from 0 LPM to 2.25 LPM and then to 3.2 LPM, the stator winding temperature and jacket cover temperature significantly dropped from 70 °C to 55 °C and further to 53 °C, and from 40 °C to 26 °C and then to 25 °C, respectively.

Temperatures at position T_5, T_6, T_7, and T_8 were 24.91 °C, 25.78 °C, 26 °C, and 26.03 °C, respectively. It was observed that the temperature gradually increases from the inlet to the outlet due to the circular topology of the SWJ. Despite conducting experiments at three different volume flow rates, the heat generation of the motor, calculated as in Eq. (1), remains approximately consistent at 100 A, 150 A, and 200 A, calculating 30 W, 65 W, and 110 W, respectively. The heat transfer coefficient, as determined by Eq. (2), was approximately 75 W/m²-K. Therefore, the computed experimental results can be confidently employed as input parameters for the simulation process.

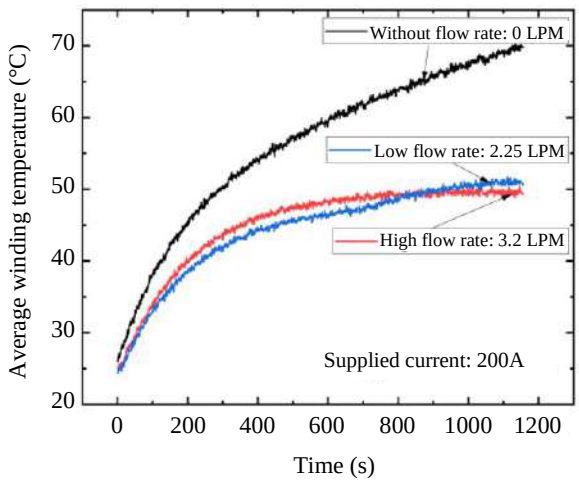

Fig. 11. Average winding time-dependent temperature.

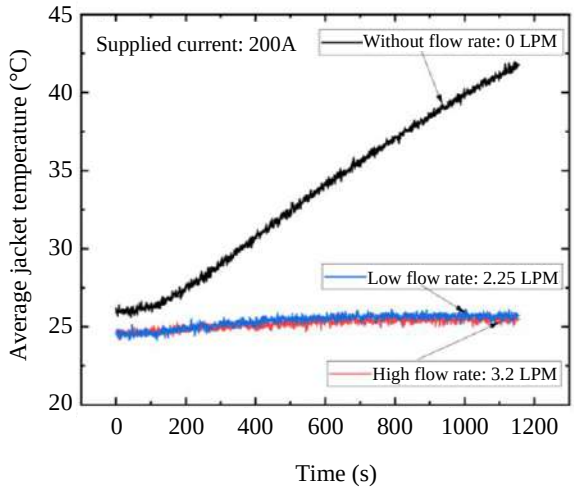

Fig. 12. Average jacket time-dependent temperature.

4.3 Temperature Fluctuation of the Motor

Fig. 11 and Fig. 12 reveal fluctuations in both the stator winding and jacket temperatures. Yang et al. [13] study similarly appeared this phenomenon and explained with thermocouple implementations. However, Fig. 13 demonstrated that temperature fluctuations were impacted by the supplied current and flow rate.

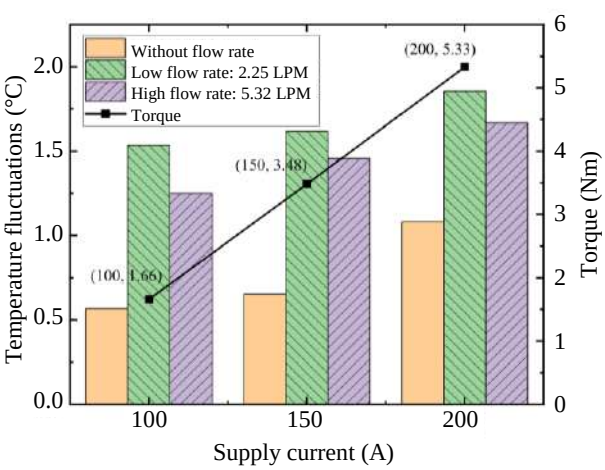

Fig. 13. The stator winding temperature oscillation.

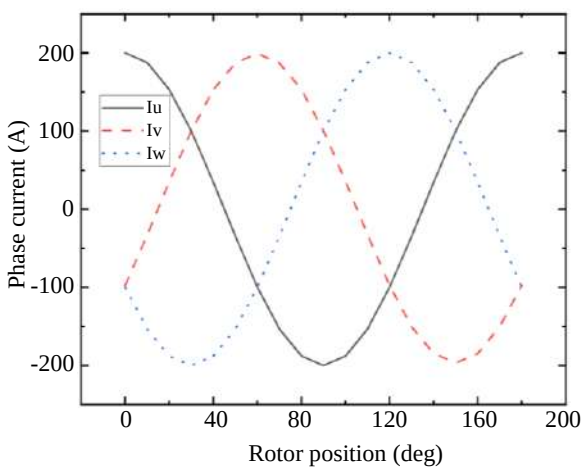

Fig. 14. Three-phase electrical supply with a peak current of 200 A.

Remarkably, the lowest temperature fluctuations consistently occur when there was no flow rate. As the supplied current increases, the temperature oscillations also rise. Specifically, the supplied currents of 100 A, 150 A, and 200 A, the temperature fluctuations without flow rate were approximately 0.57 °C, 0.65 °C, and 1.08 °C, respectively. This can be explained by the increasing current oscillation of the three-phase current. In particular, for a peak current of 200 A, the three-phase alternating current oscillates with a magnitude of 100 A, as shown in Fig. 14.

Conversely, when the flow rate increases, the temperature oscillations diminish. When a current level was 200 A and the flow rate was increases from 2.25 LPM to 5.32 LPM, the temperature fluctuation decreases from 1.86 °C to 1.67 °C. This result exhibits similarity to findings in the study conducted by Hirasawa et al. [20], where it was explained due to the increase in the flow volume of water.

Braslavsky et al. [21] research concluded that temperature oscillations accelerate the aging process of the stator winding insulation. This poses a subsequent challenge when attempting to enhance the motor torque after reducing its maximum temperature.

4.4 Effect of Flow Rate on the Cooling Jacket Model

From Fig. 11 and Fig. 12, it can be observed that as the flow rate increases from 0 LPM to 2.25 LPM, the winding and jacket temperature significantly decrease. However, as the flow rate was raised from 2.25 LPM to 3.2 LPM, the temperature reduction was slight. In order to clarify the temperature field variation with the flow rate, simulations were carried out using a smaller flow rate step, at a supplied current of 200 A. From Fig. 15, it can be observed that the maximum jacket temperature decreases as the flow rate increases within the range of 1-5 LPM, flow rate step of 1 LPM.

At a flow rate of 1 LPM, the SWJ temperature was 26.96 °C, and the LWJ temperature was 26.18 °C. As the flow rate grew to 5 LPM, the SWJ temperature dropped to 25 °C, and the LWJ temperature declined to 24.79 °C. With each step of flow rate increment, the SWJ and LWJ temperatures went down by 1.29 °C, 0.38 °C, 0.19 °C, and 0.1 °C, and by 0.88 °C, 0.29 °C, 0.14 °C, and 0.08 °C, respectively.

At 2 LPM, the SWJ and LWJ temperatures plummeted compared to 1 LPM which were slightly higher than the temperatures at further flow rates. In order to reduce power consumption, 2 LPM was chosen as the optimal rate.

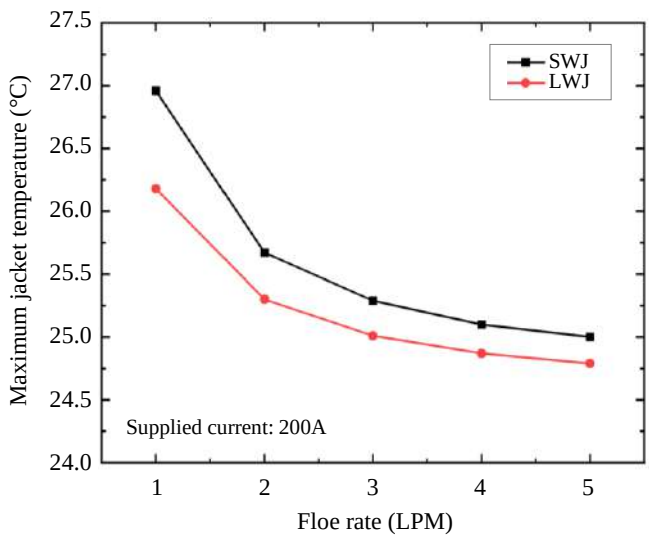

Fig. 15. Relationship between temperature and flow rate.

4.5 Effect Water Path on Temperature Distribution

The temperature distribution of the SWJ and LWJ was shown in Fig. 16 and Fig. 17, respectively. In general, both models display a progressively increasing temperature from the inlet to the outlet. However, in the SWJ model, the temperature distribution along the vertical axis of the motor differs between positions with water channels and those without. In contrast, the temperature distribution in the LWJ model was more uniform. This can be explained due to the water path of the LWJ model combining both circular and longitudinal routes. Additionally, this LWJ topology, combined and separated water channel structure, promotes a consistent water velocity within the channels.

The SWJ exhibits a larger temperature difference between the solid domain and the water domain compared to the LWJ. Therefore, according to Eq. (2), HTC of the SWJ was lower than that of the LWJ. This explained why the maximum temperature of the SWJ was higher than that of the LWJ. This assertion was supported by Silwal et al. [22] research.

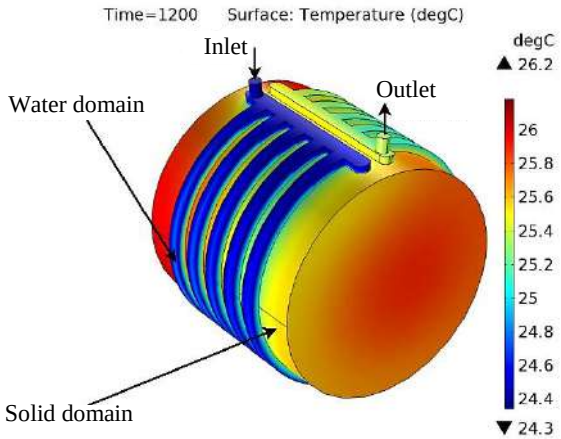

Fig. 16. Temperature distribution of SWJ.

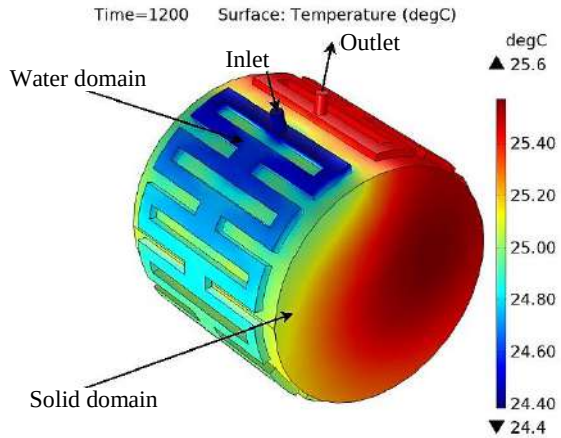

Fig. 17. Temperature distribution of LWJ.

5. Conclusions

Evaluating the impact of factors on the cooling process of the WJ for the SynRM has been investigated. Based on the results of experiments and simulations, the main conclusion can be summarized as follows:

(1) The water-cooling jacket proved highly effective in significantly reducing the temperature of both the SynRM stator winding and the jacket. Moreover, the experimental process utilized to gather data for the input parameters of the simulation was conducted reliably.

(2) Temperature fluctuation increased as the supplied current went from 100 A to 200 A. In contrast, it decreased as the flow rate rose from 2.25 LPM to 5.32 LPM. Furthermore, these temperature fluctuations reduce the insulation lifespan of the stator winding, which presents an additional challenge in enhancing motor torque after decreasing the maximum temperature.

(3) Raising the flow rate of the water within the WJ assists in reducing the maximum temperature of the motor and jacket. When the flow rate was relatively low, raising it led to a significant reduction in the maximum temperatures for both SWJ and LWJ. However, when the flow rate climbed beyond a certain value, further increments did not significantly fall the maximum motor temperature. In order to balance cooling capacity and power consumption, the flow rate was considered and chosen.

(4) The water path that combined both circular and longitudinal routes helped to achieve a more uniform temperature distribution in the longitudinal direction. However, in the circumferential direction, both models showed an increasing temperature from the inlet to the outlet. Nevertheless, the research methodology in this paper could serve as a foundation for more specialized designs. Furthermore, a longer water path enhanced the HTC of the water-cooling jacket, thereby reducing the maximum temperature.

Nomenclature

Q	Heat generation of motor, W
T_{inlet}	Inlet temperature, ºC
T_{outlet}	Outlet temperature, ºC
F_v	Volume flow rate, m^3/s
ρ	Density of water, kg/m^3
C_p	Specific heat capacity of water, J/kg-K
q	Heat flux, W/m^2
T_{inside}	Average temperature of T1, T2, T3, and T4, ℃
$T_{outside}$	Average temperature of T5, T6, T7, and T8, ℃
A	Surface area of the inner jacket

Subscripts

ICE	Internal combustion engine
EV	Electric vehicle
mcTEST	Maximum torque per ampere
WJ	Water-cooling jacket
HTC	Heat transfer coefficient
SynRM	Synchronous reluctance motor
SWJ	Short water-path jacket
LWJ	Long water-path jacket
FEM	Finite element method
T_1, T_2, T_3, and T_4	Winding temperature sensor positions
T_5, T_6, T_7, and T_8	Jacket temperature sensor positions

Acknowledgments

This work was supported from Thailand Advanced Institute of Science and Technology, Tokyo Institute of Technology, National Energy Technology Center, and National Electronics and Computer Technology Center. Additionally, the authors gratefully acknowledged the Monozukuri Degree, King Mongkut's Institute of Technology Ladkrabang funded research materials.

References

[1] La Rocca A, La Rocca S, Zou T, Liu C, Moslemin M, Gerada C, et al. Performance assessment of standard cooling strategies for hairpin windings. 2022 International Conference on Electrical Machines (ICEM); 2022 Sep 5-8; Valencia, Spain. USA: IEEE; 2022. p. 1163-1169.

[2] Cavazzuti M, Gaspari G, Pasquale S, Stalio E. Thermal management of a formula E electric motor: analysis and optimization. Appl Therm Eng. 2019;157:113733.

[3] Liang P, Chai F, Shen K, Liu W. Thermal design and optimization of a water-cooling permanent magnet synchronous in-wheel motor. The 22nd International Conference on Electrical Machines and Systems (ICEMS); 2019 Aug 11-14; Harbin, China. USa: IEEE; 2019. p. 1-6.

[4] Raj EFI, Appadurai M, Darwin S, Thanu MC. Detailed study of efficient water jacket cooling system for induction motor drive used in electric vehicle. Int J Interact Des Manuf. 2023;17:1277-1288.

[5] Wang X, Li B, Gerada D, Huang K, Stone I, Worrall S, et al. A critical review on thermal management technologies for motors in electric cars. Appl Therm Eng. 2022;201:117758.

[6] Kim C, Lee KS, Yook SJ. Effect of air-gap fans on cooling of windings in a large-capacity, high-speed induction motor. Appl Therm Eng. 2016;100:658-667.

[7] Prieto B, Satrústegui M, Elósegui I, Gil-Negrete N. Multidisciplinary analysis of a 750 kW PMSM for marine propulsion including shock loading response. IET Electr Power Appl. 2020;14(10):1974-1983.

[8] Marcolini F, De Donato G, Capponi FG, Caricchi F. Direct oil cooling of end-windings in torus-type axial-flux permanent-magnet machines. IEEE Trans Ind Appl. 2021;57(3):2378-2386.

[9] Gundabattini E, Mystkowski A, Raja Singh R, Gnanaraj SD. Water cooling, PSG, PCM, Cryogenic cooling strategies and thermal analysis (experimental and analytical) of a Permanent Magnet Synchronous Motor: a review. Sadhana. 2021;46(3):124.

[10] Wu PS, Hsieh MF, Cai WL, Liu JH, Huang YT, Caceres JF, et al. Heat transfer and thermal management of interior permanent magnet synchronous electric motor. Inventions. 2019;4(4):69.

[11] Chen W, Ju Y, Yan D, Guo L, Geng Q, Shi T. Design and optimization of dual-cycled cooling structure for fully-enclosed permanent magnet motor. Appl Therm Eng. 2019;152:338-349.

[12] Chuan H, Burke R, Wu Z. A comparative study on different cooling topologies for axial flux permanent magnet machine. 2019 IEEE Vehicle Power and Propulsion Conference (VPPC); 2019 Oct 14-17; Hanoi, Vietnam. USA: IEEE; 2019. p. 1-6.

[13] Yang X, Fatemi A, Nehl T, Hao L, Zeng W, Parrish S. Comparative study of three stator cooling jackets for electric machine of mild hybrid vehicle. 2019 IEEE International Electric Machines and Drives Conference (IEMDC); 2019 May 12-15; San Diego, USA. USA: IEEE; 2019. p. 1202-1209.

[14] Nategh S, Wallmark O, Leksell M. Thermal analysis of permanent-magnet synchronous reluctance machines. Proceedings of the 2011 14th European Conference on Power Electronics and Applications; 2011 Aug 30 - 2011 Sep 1; Birmingham, United Kingdom. USA: IEEE; 2011. p. 1-10.

[15] Herrera DB, Galvan E, Carrasco JM. Synchronous reluctance motor design based EV powertrain with inverter integrated with redundant topology. IECON 2015 - 41st Annual Conference of the IEEE Industrial Electronics Society; 2015 Nov 9-12; Yokohama, Japan. USA: IEEE; 2015. p. 003851-003856.
[16] Kerdsup B, Karukanan S. Design of motor characteristic testbed for permanent-magnet assisted synchronous reluctance motor. 2022 25th International Conference on Electrical Machines and Systems (ICEMS); 2022 Nov 29 - 2022 Dec 02; Chiang Mai, Thailand. USA: IEEE; 2022. p. 1-4.
[17] Liang P, Chai F, Shen K, Liu W. Water jacket and slot optimization of a water-cooling permanent magnet synchronous in-wheel motor. IEEE Trans Ind Appl. 2021;57(3):2431-2439.
[18] Wan Y, Li Q, Guo J, Cui S. Thermal analysis of a Gramme-ring-winding high-speed permanent-magnet motor for pulsed alternator using CFD. IET Electr Power Appl. 2020;14(11):2202-2211.
[19] Wang H, Tao T, Xu J, Mei X, Liu X, Gou P. Cooling capacity of a novel modular liquid-cooled battery thermal management system for cylindrical lithium ion batteries. Appl Therm Eng. 2020;178:115591.
[20] Hirasawa S, Kawanami T, Shirai K. Efficient cooling system using electrocaloric effect. J Electron Cool Therm Control. 2016;6(2):78-87.
[21] Braslavsky IY, Metelkov VP, Esaulkova DV, Kostylev AV. Simplified method of taking into account temperature fluctuations influence on durability of induction motors stator winding insulation. 2018 17th International Ural Conference on AC Electric Drives (ACED); 2018 Mar 26-30; Ekaterinburg, Russia. USA: IEEE; 2018. p. 1-4.
[22] Silwal B, Mohamed AH, Nonneman J, De Paepe M, Sergeant P. Assessment of different cooling techniques for reduced mechanical stress in the windings of electrical machines. Energies. 2019;12(10):1967.